Research Square

Preprints are preliminary reports that have not undergone peer review.
They should not be considered conclusive, used to inform clinical practice,
or referenced by the media as validated information.

Direct targeting of SLC7A11 by miR-143-3p promotes ferroptosis and suppresses malignancy in cervical squamous cell carcinoma

Jingwen Meng
Gulou Clinical Medical College, Nanjing Medical University
Hongyun Wang
Gulou Clinical Medical College, Nanjing Medical University
Meixia Wang
Nanjing University of Chinese Medicine
Ying Hong
hongying@nju.edu.cn

Gulou Clinical Medical College, Nanjing Medical University

Article

Keywords: RNA-seq, miR-143-3p, SLC7A11, Ferroptosis, Cervical cancer

Posted Date: August 20th, 2026

DOI: https://doi.org/10.21203/rs.3.rs-10336712/v1

License: This work is licensed under a Creative Commons Attribution 4.0 International License.
Read Full License

Additional Declarations: No competing interests reported.

Abstract

Background

Cervical cancer is a major cause of cancer-related mortality among women, and current therapeutic options remain limited. Emerging evidence suggests that targeted induction of ferroptosis represents a promising strategy for cancer management. Nevertheless, the role and underlying mechanisms of ferroptosis in early-stage cervical squamous cell carcinoma (SCC) remain unclear.

Objective

To investigate whether direct targeting of SLC7A11 by miR-143-3p promotes ferroptosis in cervical SCC and suppresses its malignant behaviour.

Methods

RNA sequencing was performed on cervical tissues obtained from three patients with SCC (stage IB, HPV16-positive) and three normal controls (HPV16-negative). Differential gene expression, functional enrichment, and protein–protein interaction network analyses were conducted to identify key microRNAs and their target genes. The expression levels of miR-143-3p and SLC7A11 in SCC and control tissues were determined using quantitative real-time polymerase chain reaction, immunohistochemical staining, and Western blotting (WB). Furthermore, the effects of miR-143-3p mimics and inhibitors on cell proliferation and ferroptosis were evaluated using Cell Counting Kit-8 and scratch assays, in combination with WB, while ferroptosis-related biochemical markers were simultaneously assessed. Finally, the role of miR-143-3p in the epithelial–mesenchymal transition (EMT) of cervical cancer cells was examined using WB and immunofluorescence.

Results

miR-143-3p was identified as a key miRNA and was significantly downregulated in SCC. In vitro experiments demonstrated that overexpression of miR-143-3p promoted ferroptosis in cervical cancer cells by suppressing SLC7A11 expression. Luciferase reporter gene assays confirmed the direct regulatory interaction between miR-143-3p and SLC7A11. Additionally, overexpression of miR-143-3p attenuated EMT in cervical cancer cells, potentially exerting an inhibitory effect on tumour metastasis.

Conclusions

In cervical cancer cells, miR-143-3p functions as a tumour suppressor and may promote ferroptosis through downregulation of SLC7A11. This regulatory mechanism influences malignant cellular

behaviour, suggesting that the miR-143-3p/SLC7A11 axis may serve as a novel therapeutic target for the treatment of cervical cancer.

Introduction

Cervical cancer is one of the most prevalent gynaecological malignancies and remains a leading cause of cancer-related mortality among women worldwide, particularly in developing countries[1–3]. Despite advances in screening, vaccination, and multimodal treatment strategies, the prognosis of patients with cervical squamous cell carcinoma (SCC)—the most common histological subtype—remains unsatisfactory once tumour progression or metastasis occurs. Current therapeutic approaches primarily rely on surgery, radiotherapy, and chemotherapy; however, drug resistance and treatment-associated toxicity continue to limit clinical efficacy[2,4]. Therefore, it is crucial to elucidate novel molecular mechanisms underlying cervical cancer progression and to identify potential therapeutic targets.

Ferroptosis is a recently characterised form of regulated cell death driven by iron-dependent lipid peroxidation and is distinct from apoptosis, necrosis, and autophagy in both morphology and molecular regulation[5,6]. Accumulating evidence indicates that ferroptosis plays a pivotal role in tumorigenesis and in responses to cancer therapy[7–9]; its induction may provide a promising strategy for overcoming therapeutic resistance in multiple cancers. Key regulators of ferroptosis include iron metabolism, lipid peroxidation pathways, and antioxidant systems. Notably, the cystine/glutamate antiporter system Xc^-, which comprises the light chain subunit SLC7A11, functions as a central suppressor of ferroptosis by maintaining intracellular glutathione (GSH) homeostasis[10,11]. Aberrant upregulation of SLC7A11 has been reported in various malignancies and is closely associated with tumour growth, metastasis, and resistance to oxidative stress[12,13]. However, the involvement of ferroptosis and its regulatory network in early-stage cervical SCC remains incompletely understood.

MicroRNAs (miRNAs) are a class of small non-coding RNAs that modulate gene expression at the post-transcriptional level and participate extensively in cancer-associated biological processes (BP), including cell proliferation, invasion, metastasis, and programmed cell death[14,15]. Although dysregulation of miRNAs has been implicated in the initiation and progression of cervical cancer, their role in the regulation of ferroptosis has only recently begun to be explored[16,17]. miR-143-3p has been established as a tumour suppressor in numerous cancers, where it regulates cell growth, migration, and epithelial–mesenchymal transition (EMT)[18,19]. Nevertheless, the contribution of miR-143-3p to the regulation of ferroptosis in cervical cancer, as well as its underlying molecular mechanisms, remains largely unknown.

In this study, we performed RNA sequencing (RNA-seq) on cervical tissues obtained from patients with early-stage cervical SCC and from normal controls, followed by integrative bioinformatic analyses to identify ferroptosis-related regulatory networks. We identified miR-143-3p as a key downregulated miRNA in cervical SCC, with SLC7A11 predicted as its target. Through in vitro functional experiments, we investigated the effects of miR-143-3p on proliferation, ferroptosis, and EMT in cervical SCC cells, while

verifying the direct regulatory interaction between miR-143-3p and SLC7A11. Our findings reveal a previously uncharacterised miR-143-3p/SLC7A11 axis that modulates ferroptosis and malignant biological behaviour in cervical cancer cells, thereby providing new insights into the molecular mechanisms of cancer progression and highlighting a potential therapeutic target for future intervention.

Materials and methods

2.1 General

This study received ethical approval from the Ethics Committee of Nanjing Drum Tower Hospital, Affiliated Hospital of Nanjing University Medical School, China (No. 2020-333-02 and No. 2026-0263-01), and was conducted in accordance with the principles of the Declaration of Helsinki. Written informed consent was obtained from all patients for experiments involving human biological samples. SiHa and HeLa cells were obtained from the Cell Bank of the Chinese Academy of Sciences. We have deposited the raw sequencing data generated in this study into the NCBI Sequence Read Archive (http://www.ncbi.nim.nih.gov/sra) with the accession number PRJNA1032265.

2.2 Bioinformatics and protein–protein interaction (PPI) network analyses

A comprehensive genome-wide mRNA expression analysis was performed using cervical tissues from patients with early-stage SCC and from normal controls. Heatmaps, volcano plots, and bubble charts were generated based on the analysed data. Whole transcriptome sequencing was performed using the Illumina HiSeq 6000. Bioinformatics methods were employed to screen differentially expressed genes (with screening criteria of |Fold change| ≥ 2 and False discovery rate < 0.05), followed by GO functional enrichment analysis and KEGG pathway enrichment analysis. Furthermore, by integrating with the ferroptosis database FerrDb, differentially expressed genes associated with ferroptosis were identified as potential key molecules. To investigate molecular targets involved in cervical cancer pathogenesis, a PPI network of ferroptosis-related genes (FRGs) was constructed using the STRING database (http://www.string-db.org/). The results were further analysed using the Network Analyzer tool in Cytoscape version 3.8.2.

2.2.1 RNA extraction

Total RNA was extracted from the tissue using miRNeasy Serum/Plasmakit according the manufacturer’s instructions. Then RNA quality was determined by Agilent2100 Pico (Agilent) and quantified using the ND-2000 (NanoDrop Technologies). Only high-quality RNA sample(OD260/280 = 1.8 ~ 2.2, OD260/230 ≥ 2.0, RQN ≥ 6.5, 28S:18S ≥ 1.0, > 3ng) was used to construct sequencing library.

2.2.2. Library preparation and sequencing

RNA purification, reverse transcription, library construction and sequencing were performed at Shanghai Majorbio Bio- pharm Biotechnology Co., Ltd. (Shanghai, China) according to the manufacturer' s instructions (Illumina, San Diego, CA). A total amount of 1 μ g total RNA per sample was used as input material for the small RNA library. Sequencing libraries were generated using SMARTer smRNA-Seq Kit for Illumina following manufacturer' s recommendations. Theactivated 5 ' and 3 ' adaptors were ligated to the total RNA, respectively. Then the adaptor- ligated RNA was transcribed into first- strand cDNA by using reverse transcriptase and random primer. A PCR reaction was performed using primers complementary for 11–12 cycles, fragments of appropriate size were isolated by a 6% Novex TBE PAGE gel. After quantified by Qubit 4. 0, single- end RNA- seq sequencing library was sequenced with the Illumina NovaSeq 6000 Xplus sequencer.

2.2.3.Quality control and reads mapping

Raw data (raw reads) of fastq format were firstly processed through fastp[20] with default parameters. After this step, clean data(clean reads) were obtained by removing 3 ' end adapter, reads containing ploy-N, low-quality bases (Sanger base quality of < 20) of the 3' end and sequencing adapters from raw data with the fastx toolkit software. All identical sequences of sizes ranging from 18 to 32 nt were counted and eliminated from the initial data set. Bowtie[21] was used to annotate the chromosomal location against the reference genome data.

2.2.4. Identification of miRNAs and Differential expression analysis

The mapped small RNA tags were firstly used to identifying known miRNA with miRBase2 2. 0 database (http://www.mirbase.org/) as reference. Then the rest of tags were aligned with Rfam database and Repbase database to remove ribosomal RNA (rRNA), transfer RNA (tRNA), small nuclear RNA (snRNA), small nucleolar RNA(snoRNA) and other ncRNA and repeats. The unannotated tags were predicted to be and identified as novel miRNAs using mirdeep2 [22] software, according to the tag positions in the genome and their hairpin structures. The expression level of each miRNA was calculated according to the transcripts per million reads (TPM) method. Differential expression analysis was performed using the DESeq2[23] or DEGseq[24]. DEGs with |log2FC| ≥ 1 and FDR ≤ 0.05 (DESeq2) or FDR ≤ 0.001 (DEGseq) were considered to be significantly different expressed genes.

2.2.5. Target gene predictions of miRNAs

Target gene predictions of miRNAs were performed with miRanda[25] for animal or psRobot[26] for plant. The predicted target genes were annotated with GO (http://www.geneontology.org/) and KEGG (http://www.genome.jp/kegg/) database. Functional- enrichment analysis including GO and KEGG were performed to identify which targets were significantly enriched in GO terms and metabolic pathways at P- adjust ≤ 0. 05 compared with the whole- ref genes background. GO functional enrichment and KEGG pathway analysis were carried out by Goatools and KOBAS[27], respectively.

2.3 Gene Ontology (GO) functional annotation and Kyoto Encyclopedia of Genes and Genomes (KEGG) pathway enrichment analysis

To determine the biological functions and pathways associated with cervical cancer-related targets, GO and KEGG pathway enrichment analyses were performed using the DAVID database. GO annotation included BP, cellular components, and molecular functions, whereas KEGG analysis identified pathways relevant to pathological mechanisms. Enrichment results were visualised, and three public databases (TargetScan, miRDB, and miRWalk) were used to predict potential miRNAs regulating SLC7A11 expression. The copyright of the KEGG pathway database belongs to the Kanehisa Laboratory, and we have obtained their formal permission.

2.4 Cell culture

SiHa and HeLa cells were cultured in Dulbecco's modified Eagle's medium and RPMI 1640 medium, respectively, supplemented with 10% fetal bovine serum (FBS) and 1% penicillin–streptomycin. Both cell lines were maintained at 37°C in a humidified atmosphere containing 5% CO_2, and the culture medium was replaced every 2–3 days.

2.5 Polymerase chain reaction (PCR)

DNA was extracted from tissues and cells using the EasyPure® Genomic DNA Kit (without RNase A) according to the manufacturer's instructions. DNA concentration was measured using a microvolume UV spectrophotometer. PCR amplification was performed using the 2× Easy Taq PCR Super Mix Kit in a 25 μL reaction mixture comprising 2 μL of DNA template, 0.5 μL of each forward and reverse primer (50 ng/μL), 12.5 μL of 2× PCR Mix, and 9.5 μL of sterile double-distilled water. Primers were designed and synthesised by Shanghai Sangon Biological Engineering Technology & Services Co., Ltd., with the following sequences: GPX4 forward: 5'-GAGGCAAGACCGAAGTAAACTAC-3', reverse: 5'-CCGAACTGGTTACACGGGAA-3'; SLC7A11 forward: 5'-AACTGCTGGTAATACGCCCC-3', reverse: 5'-GGAAAATCTGGATCCGGGCA-3'; GAPDH forward: 5'-ACGGGAAACCCATCACCAT-3', reverse: 5'-TCACAAACATGGGGGCAT-3'.

2.6 Transwell assay

For invasion assays, SiHa and HeLa cells were seeded into the upper chambers of Transwell inserts (Corning Costar Co., Cambridge, MA, USA). The upper chambers were pre-coated with Matrigel (BD Biosciences) for invasion assays. Cells were cultured in serum-free medium in the upper chamber, whereas the lower chamber contained medium supplemented with 10% FBS to promote cell migration. After 12 h, cells that had invaded or migrated to the lower surface of the membrane were fixed, stained, imaged, and counted.

2.7 Western blotting (WB)

Cells were harvested by trypsinisation and subsequently lysed using high-efficiency RIPA lysis buffer supplemented with protease inhibitors. Protein concentrations in the supernatants were measured.

Subsequently, 20–30 μg of total protein per sample was separated by SDS–PAGE and transferred onto polyvinylidene difluoride membranes using a wet transfer system (100 mA, 12 h, 4°C). The membranes were blocked with 5% non-fat milk and incubated with primary antibodies (Caspase-3: Affinity, 1:1000 dilution, cat. no. AF6311; GPX4: Affinity, 1:1000 dilution, cat. no. DF6701; SLC7A11: Affinity, 1:1000 dilution, cat. no. DF12509; N-cadherin: Affinity, 1:1000 dilution, cat. no. AF5239; E-cadherin: Affinity, 1:1000 dilution, cat. no. AF0131; fibronectin: Affinity, 1:1000 dilution, cat. no. AF5335; vimentin: Affinity, 1:1000 dilution, cat. no. AF7013; β-actin: Affinity, 1:1000 dilution, cat. no. AF7018). Protein expression in each group was detected using a chemiluminescence imaging system and quantified with ImageJ software. The gel/western blot (WB) obtained in the experiment is shown in Supplementary Annex 3.

2.8 Cell counting kit-8 (CCK-8) assay

SiHa and HeLa cells were seeded separately into 96-well plates. At different experimental time points, cells were transfected with miR-143-3p mimic or negative control (miR-NC) as indicated. According to the CCK-8 kit instructions (Glpbio, USA), the culture medium was replaced with fresh medium containing 10% CCK-8 reagent. After incubation for 1 h, absorbance was measured at 450 nm using a microplate reader to evaluate cell proliferation.

2.9 Transfection of miRNA mimic

Adherent cells were seeded in 24-well plates 18–24 h before transfection to achieve 50–70% confluence. Cells were then transfected with miR-NC using Lipofectamine 3000 reagent according to the manufacturer's instructions. The culture medium was replaced with 2 mL of fresh medium, and the appropriate volume of miRNA mimic complex was added. Cells were incubated at 37°C under standard culture conditions for subsequent experiments.

2.10 Immunofluorescence assay

Cells were seeded onto confocal culture dishes and processed according to the experimental protocol. Cell membranes were permeabilised with 1% Triton X-100 and blocked with goat serum for 60 min. Subsequently, cells were incubated with primary antibodies against SLC7A11 (1:100) and GPX4 (1:100), followed by fluorophore-conjugated secondary antibodies. Fluorescence images were captured using a fluorescence microscope.

2.11 Immunohistochemistry

Paraffin-embedded tissue sections were deparaffinised and rehydrated through graded ethanol and xylene. Antigen retrieval was performed at high temperature in sodium citrate buffer. Endogenous peroxidase activity was blocked, and the sections were incubated overnight at 4°C with anti-SLC7A11 antibody (1:200). Following incubation with a secondary antibody and 3,3'-diaminobenzidine staining, SLC7A11 expression in cervical tissues was visualised, and positively stained areas were quantified using ImageJ software.

2.12 Luciferase reporter assay

The predicted binding sequence of miR-143-3p was cloned into a dual-luciferase reporter plasmid (Promega, Madison, WI, USA) using a Vazyme Biotech cloning kit (Nanjing, China). The predicted binding site involved complementary base pairing between miR-143-3p (AGUAGAGU) and SLC7A11 (UCAUCUCA). When cells reached 70–80% confluence, 1 μg of the reporter plasmid was co-transfected with miR-NC into SiHa and HeLa cells. After 24 h, luciferase activity was measured using the Promega Dual-Luciferase Reporter Assay System.

2.13 Statistical analysis

Data were analysed using GraphPad Prism version 10 software. Results are presented as mean ± standard deviation. One-way analysis of variance was used for comparisons among multiple groups, whereas Student's t-test was applied for comparisons between two groups. A p value < 0.05 was considered statistically significant.

Results

3. 1 Transcriptomic profiling reveals enrichment of ferroptosis-related pathways in early-stage cervical SCC

To elucidate the pathogenesis of early-stage cervical SCC, we performed genome-wide mRNA expression profiling of cervical tumour tissues and matched normal tissues. Principal component analysis demonstrated a clear separation between the transcriptional profiles of the two groups (Fig. 1A). A total of 1,549 DEGs were identified in early-stage SCC, including 642 upregulated and 907 downregulated genes, based on the thresholds of p value < 0.05 and absolute fold change > 2 (Fig. 1B). Heatmap analysis of DEGs revealed distinct clustering of gene expression patterns following unsupervised hierarchical clustering (Fig. 1C). These DEGs were further visualised in a volcano plot (Fig. 1D). GO-BP enrichment analysis indicated significant dysregulation of processes related to EMT, reactive oxygen species and fatty acid metabolism, as well as cell migration and proliferation (Fig. 1E). KEGG pathway analysis showed that the DEGs were predominantly enriched in ferroptosis, GSH metabolism, and cell adhesion pathways (Fig. 1F). Collectively, these findings suggest that ferroptosis may play a crucial role in the pathogenesis of early-stage SCC.

3. 2 PPI network analysis identifies SLC7A11 as a central gene

A search of the FerrDb (http://www.zhounan.org/ferrdb/) database identified 236 FRGs. Venn diagram analysis revealed that 34 FRGs overlapped with the DEGs detected in early-stage SCC and were defined as dysregulated FRGs (Fig. 2A). These FRGs were further clustered using hierarchical clustering analysis (Fig. 2B). A PPI network constructed using the STRING database (http://www.string-db.org/) (Fig. 2C) identified SLC7A11 as a hub gene. In addition, RNA-seq data indicated significant upregulation of SLC7A11 mRNA (approximately 5.14-fold) in cervical tissues from patients with early-stage SCC (Fig. 2D). GO (Fig. 2E) and KEGG (Fig. 2F) enrichment analyses of FRGs demonstrated predominant

enrichment in pathways associated with ferroptosis, fatty acid metabolism, and response to viral infection. Collectively, these results underscore a potential role of SLC7A11 in modulating ferroptosis in early-stage cervical SCC.

3. 3 SLC7A11 is a predicted target of miR-143-3p

To investigate the potential involvement of miRNAs in early-stage cervical SCC, differentially expressed miRNAs (DEmiRs) were identified using thresholds of p value < 0.05 and absolute fold change > 2. These DEmiRs were visualised in a heatmap and volcano plot (Fig. 3A and B). Three public databases (TargetScan, miRDB, and miRWalk) were used to predict candidate DEmiRs that may regulate SLC7A11; miR-143-3p was identified as the only DEmiR common to all three databases (Fig. 3C). RNA-seq analysis further revealed marked downregulation of miR-143-3p expression (approximately 7.79-fold) in cervical tissue samples. In addition, a putative binding site for miR-143-3p was predicted within the 3'-untranslated region (3'-UTR) of SLC7A11 (Fig. 3E). Overall, these findings indicate that miR-143-3p may directly target SLC7A11 in early-stage cervical SCC.

3. 4 SLC7A11 and miR-143-3p are dysregulated in clinical samples from early-stage cervical SCC

Next, we validated the expression of SLC7A11 and miR-143-3p in cervical tissues from patients with early-stage SCC and matched normal samples. Compared with controls, SLC7A11 mRNA levels were significantly increased (approximately 4.50-fold) (Fig. 4A), whereas miR-143-3p expression was markedly decreased (approximately 3.48-fold) (Fig. 4B) in cervical tissue samples. Correlation analysis revealed a negative association between SLC7A11 mRNA levels and miR-143-3p expression in early-stage SCC tissues (Fig. 4C). Immunohistochemical staining further demonstrated a pronounced elevation of SLC7A11 expression in cervical tumour tissues (Fig. 4D). Collectively, these findings indicate that SLC7A11 and miR-143-3p are aberrantly expressed in early-stage cervical SCC.

3. 5 miR-143-3p directly targets SLC7A11

To determine whether SLC7A11 is a direct target of miR-143-3p, the effects of miR-143-3p overexpression or inhibition on SLC7A11 mRNA levels were examined using quantitative PCR (qPCR) (Fig. 5A and D). In both HeLa and SiHa cells, SLC7A11 expression was significantly reduced following miR-143-3p overexpression and significantly increased following miR-143-3p inhibition (Fig. 5B and E). WB analysis demonstrated consistent changes at the protein level (Fig. 5C, F, G, and H), and immunofluorescence staining further confirmed modulation of SLC7A11 expression in response to altered miR-143-3p levels (Fig. 5I). Bioinformatic analysis predicted SLC7A11 as a potential target of miR-143-3p, supported by a highly conserved binding site for the miR-143-3p seed sequence located within the 3'-untranslated region (3'-UTR) of SLC7A11 mRNA (Fig. 5J). To verify this direct targeting

hypothesis, luciferase reporter constructs containing either the wild-type SLC7A11 3'-UTR (WT) harbouring the miR-143-3p binding site or a mutant 3'-UTR (MUT) were generated. Compared with the negative control, miR-143-3p significantly inhibited luciferase activity of the SLC7A11-3'-UTR-WT reporter but had no significant effect on the MUT reporter in both SiHa and HeLa cells (Fig. 5K and L). Collectively, these results establish SLC7A11 as a direct target of miR-143-3p in early-stage SCC.

3. 6 miR-143-3p induces ferroptosis in cervical cancer cells

To explore the involvement of miR-143-3p in promoting ferroptosis in early-stage SCC, gain-of-function experiments were performed in cervical cancer cell lines. Transfection of two cell lines with miR-143-3p mimics, followed by cell viability assays, revealed that miR-143-3p overexpression significantly reduced cell viability in both cell lines. Notably, treatment with Fer-1 (a ferroptosis inhibitor), but not Nec-1 (a necroptosis inhibitor) or Z-VAD-FMK (a pan-caspase inhibitor of apoptosis), attenuated the miR-143-3p-induced reduction in cell viability (Fig. 6A and D). qPCR analysis showed that GPX4 and SLC7A11 mRNA levels were markedly decreased following transfection with miR-143-3p mimics (Fig. 6B and E). Consistently, WB analysis demonstrated similar changes at the protein level (Fig. 6C, F, and G). In contrast, no significant alteration in caspase-3 protein levels, a marker of apoptosis, was observed (Fig. 6C, F, and G). These findings indicate that miR-143-3p promotes ferroptosis rather than necroptosis or apoptosis in cervical cancer cells. Because lipid peroxidation and GSH depletion are two key events in ferroptosis, we further examined whether miR-143-3p regulates these processes. Overexpression of miR-143-3p significantly increased malondialdehyde, a major end product of lipid peroxidation, while concomitantly reducing intracellular GSH levels in cervical cancer cells (Fig. 6H–K). Collectively, these results suggest that miR-143-3p functions as an inducer of ferroptosis.

3. 7 miR-143-3p downregulation inhibits erastin-induced ferroptosis in cervical cancer cells

To elucidate the role of miR-143-3p in the modulation of ferroptosis, erastin (a ferroptosis inducer) was used to trigger ferroptotic damage in vitro. CCK-8 assays demonstrated that erastin significantly suppressed cell viability in cervical cancer cell lines (Fig. 7A). qPCR analysis showed a marked reduction in GPX4 and SLC7A11 mRNA levels following erastin-induced ferroptosis (Fig. 7B and C). In contrast, inhibition of miR-143-3p expression significantly attenuated the erastin-induced downregulation of GPX4 and SLC7A11 (Fig. 7B and C). WB analysis corroborated these findings at the protein level (Fig. 7D–G). Immunofluorescence staining further confirmed upregulation of GPX4 following miR-143-3p inhibition (Fig. 7H). Collectively, these findings indicate that miR-143-3p downregulation partially attenuates erastin-induced ferroptosis.

3. 8 Ferroptosis inhibits EMT in cervical cancer cells

Tumour metastasis is a critical feature of malignant progression in cervical cancer and is predominantly driven by EMT. GO enrichment analysis of all DEGs revealed significant dysregulation of BP related to epithelial cell polarity and mesenchymal cell migration (Fig. 1E), suggesting that epithelial cells in early-stage SCC may exhibit a propensity for EMT. GO and KEGG analyses further indicated that upregulated genes in early-stage SCC were mainly enriched in pathways associated with metal ion transport, epithelial cell differentiation, and cell adhesion (Fig. 8A and C). Conversely, downregulated genes were associated with keratinisation, arachidonic acid metabolism, and cell adhesion molecules (Fig. 8B and D). To investigate the relationship between miR-143-3p and EMT in cervical cancer, the expression of EMT-related proteins was examined in SiHa and HeLa cells 48 h following transfection with miR-143-3p mimic or inhibitor. WB analysis demonstrated a marked increase in mesenchymal markers (N-cadherin, fibronectin, and vimentin) and a reduction in the epithelial marker E-cadherin in cells treated with the miR-143-3p inhibitor (Fig. 8E and F). In contrast, transfection with the miR-143-3p mimic produced the opposite effect (Fig. 8E and F). Transwell assays showed a significant decrease in cell migration following transfection with the miR-143-3p mimic (Fig. 8G). Consistently, immunofluorescence staining further confirmed the altered expression of EMT-related proteins (Fig. 8H). These findings indicate that miR-143-3p functions as an inhibitor of EMT in cervical cancer cells.

Discussion

Cervical SCC arises within a distinct biological context characterised by persistent high-risk HPV infection, chronic inflammation, and sustained oxidative stress—conditions that impose strong selective pressure on cervical epithelial cells during malignant transformation[1,4,28]. Although previous studies of advanced cervical cancer have emphasised genomic instability and immune evasion, considerably less is known about how early-stage tumours adapt to oxidative stress through regulated cell death mechanisms. In this context, ferroptosis is particularly relevant, as it reflects the balance between lipid peroxidation and antioxidant defense[29]. The present study provides evidence that ferroptosis-related pathways are transcriptionally remodelled in early-stage cervical SCC, supporting the notion that suppression of ferroptotic vulnerability is not merely a late by-product of tumour progression but rather an early adaptive feature of cervical carcinogenesis. Within this framework, SLC7A11 emerges as a key regulatory node[13,30]. As the functional subunit of the cystine/glutamate antiporter system Xc^-, SLC7A11 sustains GSH synthesis and inhibits lipid peroxidation, thereby increasing the threshold for ferroptotic cell death. The upregulation of SLC7A11 observed in early-stage SCC is therefore likely to be functionally significant, enabling emerging tumour cells to stabilise antioxidant defences and survive under persistent redox stress. This observation is consistent with the hypothesis that resistance to ferroptosis can be established early during tumour evolution.

The roles of various miRNAs in the progression of cervical lesions are diverse, and different miRNAs exert distinct effects on tumour invasion and metastasis[,31,32,33.34].

A key mechanistic insight of this study is the identification of miR-143-3p as a post-transcriptional regulator linking early transcriptomic alterations to ferroptosis susceptibility in cervical cancer cells.

Although miR-143-3p[19,35] has been widely described as a tumour-suppressive miRNA in cervical cancer, its role in the regulation of ferroptosis remains unclear. The inverse relationship between miR-143-3p and SLC7A11 observed in cervical tissues, together with direct targeting of the SLC7A11 3'-UTR and consistent functional effects in vitro, supports a conceptual model in which loss of miR-143-3p during early tumorigenesis relieves repression of a central redox checkpoint, thereby reinforcing antioxidant defences and increasing the threshold for ferroptotic cell death. Importantly, this mechanism aligns with a broader paradigm in cancer biology whereby miRNAs fine-tune stress-adaptive pathways rather than functioning as binary switches.

Furthermore, this study advances the field by linking the adaptive ferroptosis-resistant state to a defined post-transcriptional regulatory mechanism. The inverse relationship between miR-143-3p and SLC7A11 observed at the tissue level, together with direct targeting of the SLC7A11 3'-UTR and consistent functional effects across cervical cancer cell lines, positions the miR-143-3p/SLC7A11 axis as a mechanistic bridge between transcriptomic alterations and ferroptosis susceptibility[36]. Conceptually, loss of miR-143-3p during cervical tumorigenesis may relieve post-transcriptional repression of SLC7A11, thereby enabling sustained antioxidant buffering and increasing the threshold for ferroptotic cell death. This framework is consistent with a broader paradigm in ferroptosis research in which miRNAs function as fine-tuners of redox checkpoints rather than binary on–off switches.

Beyond cell survival, modulation of EMT-associated phenotypes by miR-143-3p suggests that ferroptosis resistance and malignant plasticity are likely coordinated through a shared redox infrastructure [3,37]. EMT is increasingly recognised as a redox- and metabolism-sensitive process that requires enhanced antioxidant capacity to sustain cytoskeletal remodelling and migratory behaviour [38]. In cervical SCC, where local invasion and disease progression are clinically decisive, SLC7A11-mediated redox buffering may therefore serve a dual function: suppressing ferroptosis while facilitating EMT-associated phenotypic flexibility [38]. Rather than implying a strictly linear relationship, these findings support a co-regulatory model in which ferroptosis susceptibility and EMT are jointly shaped by redox remodelling downstream of miR-143-3p/SLC7A11 signalling.

Several limitations of this study should be acknowledged. First, the transcriptomic analysis was performed in a relatively small cohort, which limits statistical power and increases susceptibility to inter-individual variability. Second, differences in HPV status between tumour and control tissues may partially confound the observed gene expression patterns, as HPV infection itself can influence oxidative stress responses and immune-related pathways. Third, the functional analyses were restricted to in vitro models, and the absence of in vivo validation precludes definitive conclusions regarding tumour growth, invasion, or therapeutic efficacy in an organismal context. Finally, although SLC7A11 was validated as a direct target of miR-143-3p, additional downstream effectors of miR-143-3p are also likely to contribute to the observed phenotypes, particularly with respect to EMT regulation.

Moreover, systematic interrogation of additional miR-143-3p targets and their interactions with redox and metabolic pathways may further clarify how ferroptosis regulation is integrated with malignant plasticity

in cervical cancer. Collectively, these findings position ferroptosis resistance as an early and biologically adaptive feature of cervical SCC and identify the miR-143-3p/SLC7A11 axis as a promising mechanistic bridge between the unique oxidative environment of cervical carcinogenesis and susceptibility to ferroptosis.

Conclusion

In summary, this study demonstrates that ferroptosis-related regulatory alterations occur early in cervical SCC and establishes the miR-143-3p/SLC7A11 axis as a critical modulator of this process. Loss of miR-143-3p promotes ferroptosis resistance through upregulation of SLC7A11, whereas restoration of miR-143-3p sensitises cervical cancer cells to ferroptosis and suppresses EMT-associated malignant behaviours. These findings provide mechanistic insight into the role of redox regulation in early cervical carcinogenesis and highlight that targeting the miR-143-3p/SLC7A11 axis may represent a promising therapeutic strategy for cervical cancer.

Declarations

Conflict of Interests

No conflict of interest reported by all the authors.

Ethics approval and consent to participate

The study was approved by the Medical Ethics Committee of Drum Tower Hospital Affiliated to Nanjing University Medical School (Approval No.: 2020-333-02 and No.2026-0263-01) prior to the initiation of any research procedures. All participants provided written informed consent after being fully informed of the study purpose, procedures, potential risks, benefits, and their right to withdraw from the study at any time without prejudice to their medical care. The study was conducted in strict accordance with the ethical principles outlined in the Declaration of Helsinki and relevant national and institutional guidelines.

Funding Statement

This study was financially supported by the Scientific research project of the Institute of Science and Technology of the National Health Commission of the People's Republic of China (No.2019HX017-05) and the major collaborative innovation project of the Medical and Health Science and Technology Innovation Project of the Chinese Academy of Medical Sciences, China's 14th Five-Year Plan (No.2021-I2M-1-004).

CRediT authorship contribution statement

Prof. Ying Hong and Hongyun Wang provided the study concept and design of this paper. Jingwen Meng and Meixia Wang conducted the experiments. Jingwen Meng and Prof.Ying Hong revised the paper. The final version of the manuscript has been approved by all authors.

Data Availability

The article includes the data supporting the findings of this study.

References

1. Dijkstra, M. G. et al. Cervical cancer screening: on the way to a shift from cytology to full molecular screening. *Ann. Oncol.* **25** (5), 927–935. 10.1093/annonc/mdt538 (2014).
2. Guo, W., Dai, L. & Qiu, L. T cell subsets in cervical cancer tumor microenvironment: advances and therapeutic opportunities. *Front. Immunol.* **16** (1612032). 10.3389/fimmu.2025.1612032 (2025).
3. Armstrong, L., Willoughby, C. E. & McKenna, D. J. Targeting of AKT1 by miR-143-3p Suppresses Epithelial-to-Mesenchymal Transition in Prostate Cancer. *Cells* **12** (18). 10.3390/cells12182207 (2023).
4. Gardner, U. G. & Viswanathan, A. N. Management of Stage IVB Cervical Cancer Including the Role of Radiotherapy. *Curr. Treat. Options Oncol.* **26** (6), 524–532. 10.1007/s11864-025-01325-5 (2025).
5. Dixon, S. J. & Olzmann, J. A. The cell biology of ferroptosis. *Nat. Rev. Mol. Cell. Biol.* **25** (6), 424–442. 10.1038/s41580-024-00703-5 (2024).
6. Lei, G., Zhuang, L. & Gan, B. The roles of ferroptosis in cancer: Tumor suppression, tumor microenvironment, and therapeutic interventions. *Cancer Cell.* **42** (4), 513–534. 10.1016/j.ccell.2024.03.011 (2024).
7. Zhou, Q. et al. Ferroptosis in cancer: From molecular mechanisms to therapeutic strategies. *Signal. Transduct. Target. Ther.* **9** (1), 55. 10.1038/s41392-024-01769-5 (2024).
8. Mou, Y. et al. Ferroptosis, a new form of cell death: opportunities and challenges in cancer. *J. Hematol. Oncol.* **12** (1), 34. 10.1186/s13045-019-0720-y (2019).
9. Wang, Y. et al. Overcoming cancer chemotherapy resistance by the induction of ferroptosis. *Drug Resist. Updat*. **66** (100916). 10.1016/j.drup.2022.100916 (2022).
10. Gong, J. et al. TRIM21-Promoted FSP1 Plasma Membrane Translocation Confers Ferroptosis Resistance in Human Cancers. *Adv. Sci. (Weinh)*. **10** (29), e2302318. 10.1002/advs.202302318 (2023).
11. Jinson, S. et al. Iron, lipid peroxidation, and ferroptosis play pathogenic roles in atherosclerosis. *Cardiovasc. Res.* **121** (1), 44–61. 10.1093/cvr/cvae270 (2025).
12. Zhang, Y. et al. CircTTC13 promotes sorafenib resistance in hepatocellular carcinoma through the inhibition of ferroptosis by targeting the miR-513a-5p/SLC7A11 axis. *Mol. Cancer*. **24** (1), 32. 10.1186/s12943-024-02224-3 (2025).

13. He, F. et al. ATF4 suppresses hepatocarcinogenesis by inducing SLC7A11 (xCT) to block stress-related ferroptosis. *J. Hepatol.* **79** (2), 362–377. 10.1016/j.jhep.2023.03.016 (2023).
14. Tay, F. C. et al. Using artificial microRNA sponges to achieve microRNA loss-of-function in cancer cells. *Adv. Drug Deliv Rev.* **81**, 117–127. 10.1016/j.addr.2014.05.010 (2014).
15. Dragomir, M. P., Knutsen, E. & Calin, G. A. Classical and noncanonical functions of miRNAs in cancers. *Trends Genet.* **38** (4), 379–394. 10.1016/j.tig.2021.10.002 (2021).
16. Huang, X. et al. Dissecting miRNA signature in colorectal cancer progression and metastasis. *Cancer Lett.* **501**, 66–82. 10.1016/j.canlet.2020.12.025 (2020).
17. Melo, S. A. & Esteller, M. Disruption of microRNA nuclear transport in human cancer. *Semin Cancer Biol.* **27**, 46–51. 10.1016/j.semcancer.2014.02.012 (2014).
18. Rodríguez, M. et al. Identification of non-invasive miRNAs biomarkers for prostate cancer by deep sequencing analysis of urinary exosomes. *Mol. Cancer*. **16** (1), 156. 10.1186/s12943-017-0726-4 (2017).
19. Song, L-N. et al. Hsa_circ_0003998 promotes epithelial to mesenchymal transition of hepatocellular carcinoma by sponging miR-143-3p and PCBP1. *J. Exp. Clin. Cancer Res.* **39** (1), 114. 10.1186/s13046-020-01576-0 (2020).
20. Chen, S. et al. fastp: an ultra-fast all-in-one FASTQ preprocessor, (2018).
21. Langmead, B. & Salzberg, S. L. Fast gapped- read alignment with Bowtie 2 [J]. *Nat. Methods*. **9** (4), 357–359 (2012).
22. Friedlander, M. R., Mackowiak, S. D., Li, N., Chen, W. & Rajewsky, N. miRDeep2 accurately identifies known and hundreds of novel microRNA genes in seven animal clades. *Nucleic Acids Res.* **40**, 37–52 (2011).
23. Love, M. I., Huber, W. & Anders, S. Moderated estimation of fold change and dispersion for RNA-seq data with DESeq2[J]. *Genome Biol.* **15** (12), 550 (2014).
24. Wang, L. et al. DEGseq: an R package for identifying differentially expressed genes from RNA-seq data[J]. *Bioinformatics* **26** (1), 136–138 (2009).
25. Enright, A. J. et al. MicroRNA targets in Drosophila. *Genome Biol.* **5**, R1 (2003).
26. Wu, H. J., Ma, Y. K., Chen, T., Wang, M. & Wang, X. J. PsRobot: a web- based plant small RNA meta-analysis toolbox. *Nucleic Acids Res.* **40**, W22–W28 (2012).
27. Xie, C. et al. KOBAS 2.0: a web server for annotation and identification of enriched pathways and diseases. *Nucleic Acids Res.* **39**, W316–W322 (2011).
28. Voelker, R. A. *Cerv. Cancer Screen. JAMA* ;**330**(20):2030, doi:10.1001/jama.2023.21987 (2023).
29. Jiang, X., Stockwell, B. R. & Conrad, M. Ferroptosis: mechanisms, biology and role in disease. *Nat. Rev. Mol. Cell. Biol.* **22** (4), 266–282. 10.1038/s41580-020-00324-8 (2021).
30. Shi, C-J. et al. 5-methylcytosine methylation of MALAT1 promotes resistance to sorafenib in hepatocellular carcinoma through ELAVL1/SLC7A11-mediated ferroptosis. *Drug Resist. Updat*. **78** (101181). 10.1016/j.drup.2024.101181 (2024).

31. Xu, X. et al. Zhou H*. Transferrin receptor-involved HIF-1 signaling pathway in cervical cancer. *Cancer Gene Ther.* **17** 10.1038/s41417-019-0078-x (2019 Jan).
32. Wang, M., Meng, J. & Hu, H. W. H. Ying Hong*. Atractylodes macrocephala III suppresses EMT in cervical cancer by regulating IGF2BP3 through ETV5. *J. Cell. Mol. Med.* **28**, e18081 (2024).
33. Wang, H., Zhang, D., Chen, Q. & Hong, Y. Plasma expression of miRNA-21, – 214, -34a,and – 200a in patients with persistent HPV infection and cervical lesions. *BMC Cancer*. **19** (1), 986. 10.1186/s12885-019-6066-6 (2019).
34. Xu, J. et al. The inhibition of miR-126 in cell migration and invasion of cervical cancer through regulating ZEB1. *Hereditas* **156**, 11. 10.1186/s41065-019-0087-7. (2019). eCollection 2019. PubMed PMID: 31007650; PubMed Central PMCID: PMC6456986.
35. Fan, H. et al. Long non-coding RNA CCDC144NL-AS1 sponges miR-143-3p and regulates MAP3K7 by acting as a competing endogenous RNA in gastric cancer. *Cell. Death Dis.* **11** (7), 521. 10.1038/s41419-020-02740-2 (2020).
36. Wang, S. et al. CircPVT1 facilitates the progression of oral squamous cell carcinoma by regulating miR-143-3p/SLC7A11 axis through MAPK signaling pathway. *Funct. Integr. Genomics*. **22** (5), 891–903. 10.1007/s10142-022-00865-5 (2022).
37. Chen, R. et al. LncRNA UCC promotes epithelial-mesenchymal transition via the miR-143-3p/SOX5 axis in non-small-cell lung cancer. *Lab. Invest.* **101** (9), 1153–1165. 10.1038/s41374-021-00586-6 (2021).
38. Zhang, X. et al. Hypoxic BMSC-derived exosomal miRNAs promote metastasis of lung cancer cells via STAT3-induced EMT. *Mol. Cancer*. **18** (1), 40. 10.1186/s12943-019-0959-5 (2019).
39. Wang, X. et al. RBMS2 mediates SLC7A11 transcription-translation to regulate ferroptosis in colorectal cancer. *Free Radic Biol. Med.* **240**, 504–513. 10.1016/j.freeradbiomed.2025.08.051 (2025).

Figures

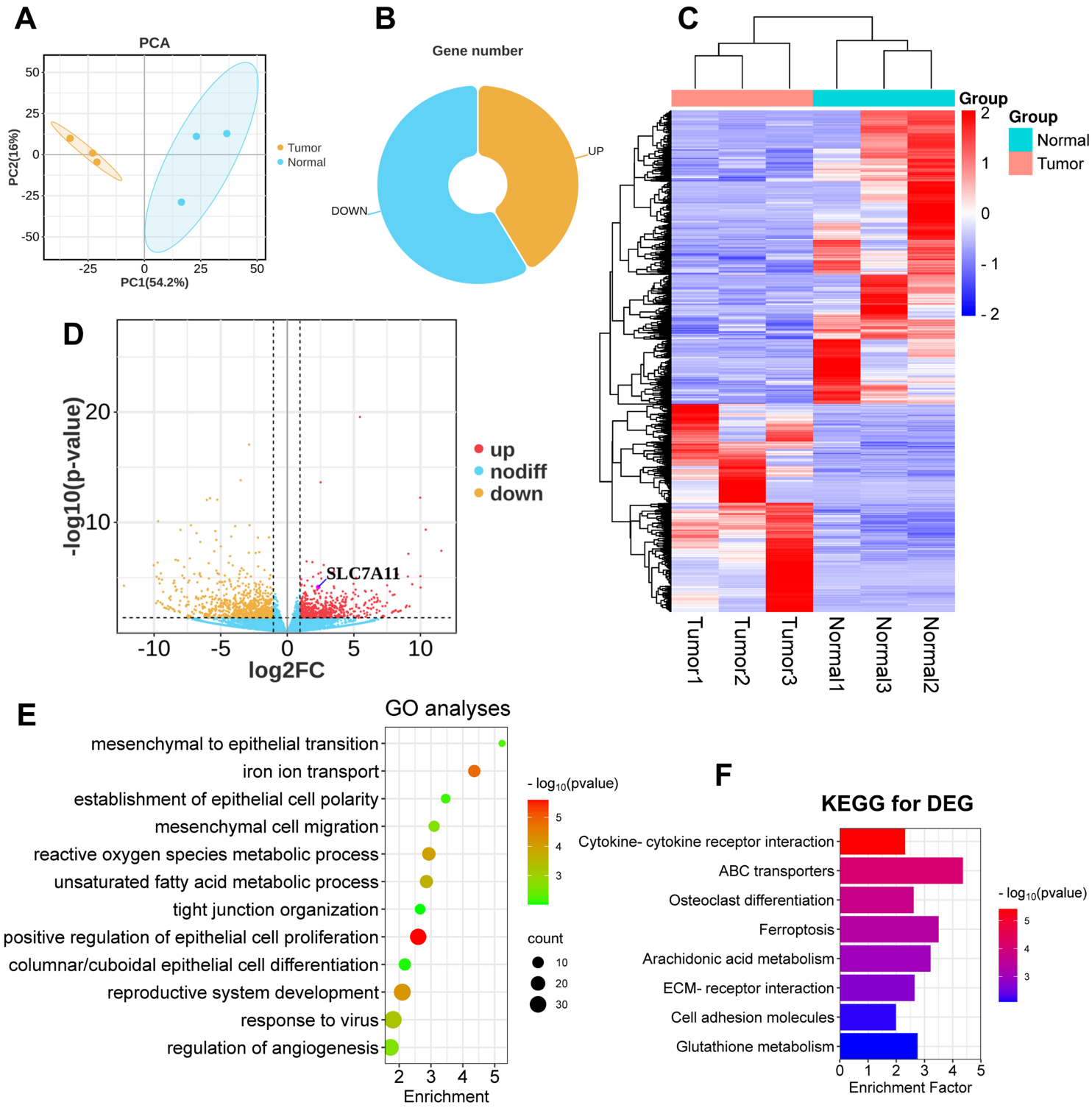


Figure 1

RNA sequencing analysis of global transcriptomic differences between early-stage cervical squamous cell carcinoma (SCC) and matched normal cervical tissues.

(A) Principal component analysis demonstrated a clear separation between the transcriptional profiles of the two groups based on global gene expression profiles. (B) Pie chart illustrating the number of upregulated and downregulated genes. (C) Heatmap with hierarchical clustering displaying differentially

expressed genes (DEGs). (D) Volcano plot of DEGs, highlighting upregulated and downregulated genes; SLC7A11 is indicated. (E) Gene Ontology (GO) analysis of DEGs, revealing significantly enriched biological processes. (F) Kyoto Encyclopedia of Genes and Genomes (KEGG) pathway analysis of DEGs, with enrichment significance denoted by −log10(p-value).

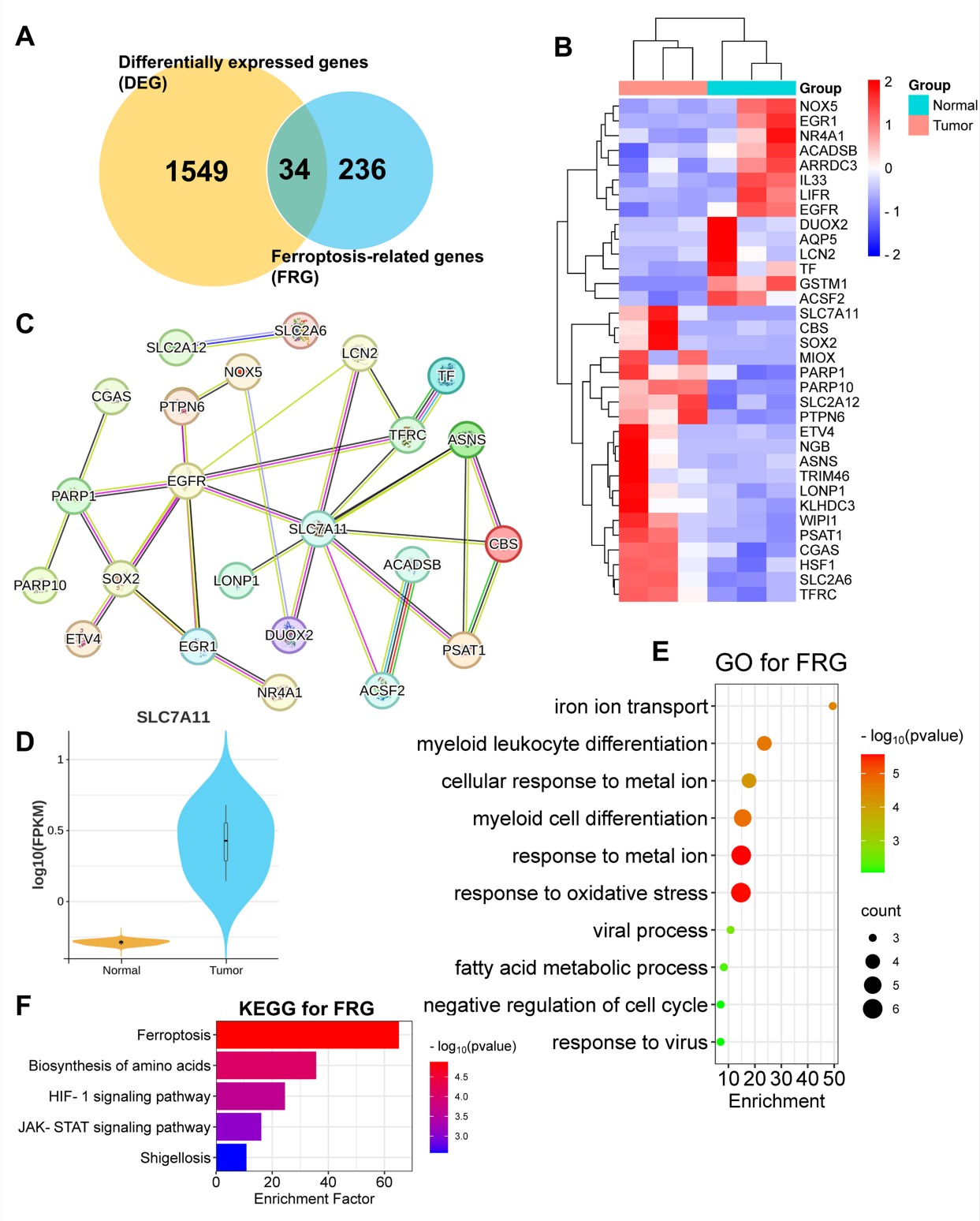


Figure 2

Identification of ferroptosis-related genes (FRGs) and pathways in early-stage cervical squamous cell carcinoma (SCC) via an integrated bioinformatic approach. (A) Venn diagram showing the overlap between differentially expressed genes (DEGs) from RNA sequencing analysis and dysregulated FRGs. (B) Heatmap with hierarchical clustering illustrating expression patterns of overlapping ferroptosis-related DEGs in SCC and normal cervical tissues. (C) A PPI network constructed using the STRING database identified SLC7A11 as a hub gene.Protein–protein interaction (PPI) network of overlapping ferroptosis-related DEGs, highlighting interactions among candidate regulatory genes. (D) Violin plot depicting the relative expression of SLC7A11 in SCC and normal cervical tissues based on transcriptomic data (log10[FPKM]). RNA-seq data indicated significant upregulation of SLC7A11 mRNA (approximately 5.14-fold) in cervical tissues from patients with early-stage SCC . (E) Gene Ontology (GO) analysis of FRGs, with significantly enriched biological processes. (F) Kyoto Encyclopedia of Genes and Genomes (KEGG) pathway analysis of FRGs. Enrichment significance is indicated by −log10(p-value), and dot size represents gene counts where applicable.

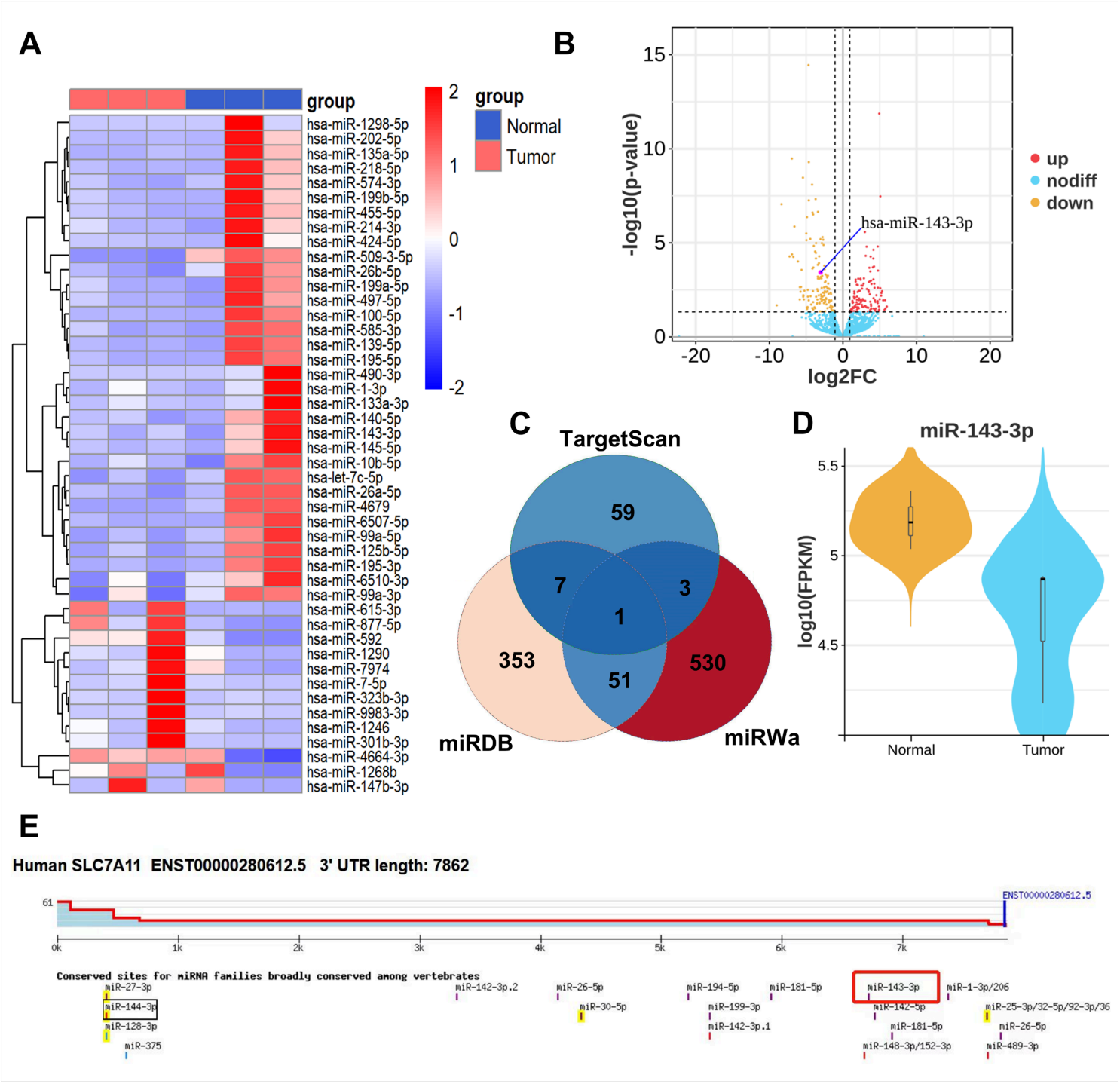


Figure 3

Integrated microRNA (miRNA) analysis and target prediction identifying key miRNAs associated with ferroptosis regulation in cervical squamous cell carcinoma (SCC). (A, B) Heatmap (A) and Volcano plot (B) showing differentially expressed miRNAs between SCC and normal cervical tissues; miR-143-3p is highlighted. (C) Venn diagram displaying the shared predicted target genes of miR-143-3p retreived from TargetScan, miRDB, and miRWalk databases. (D) Violin plot illustrating the relative expression level of miR-143-3p in SCC and normal cervical tissues, referring to transcriptomic data (log10[FPKM]). (E)

Schematic representation of miR-143-3p binding sites within the 3' untranslated region (3'UTR) of human SLC7A11 as predicted by TargetScan, with conserved sites highlighted.

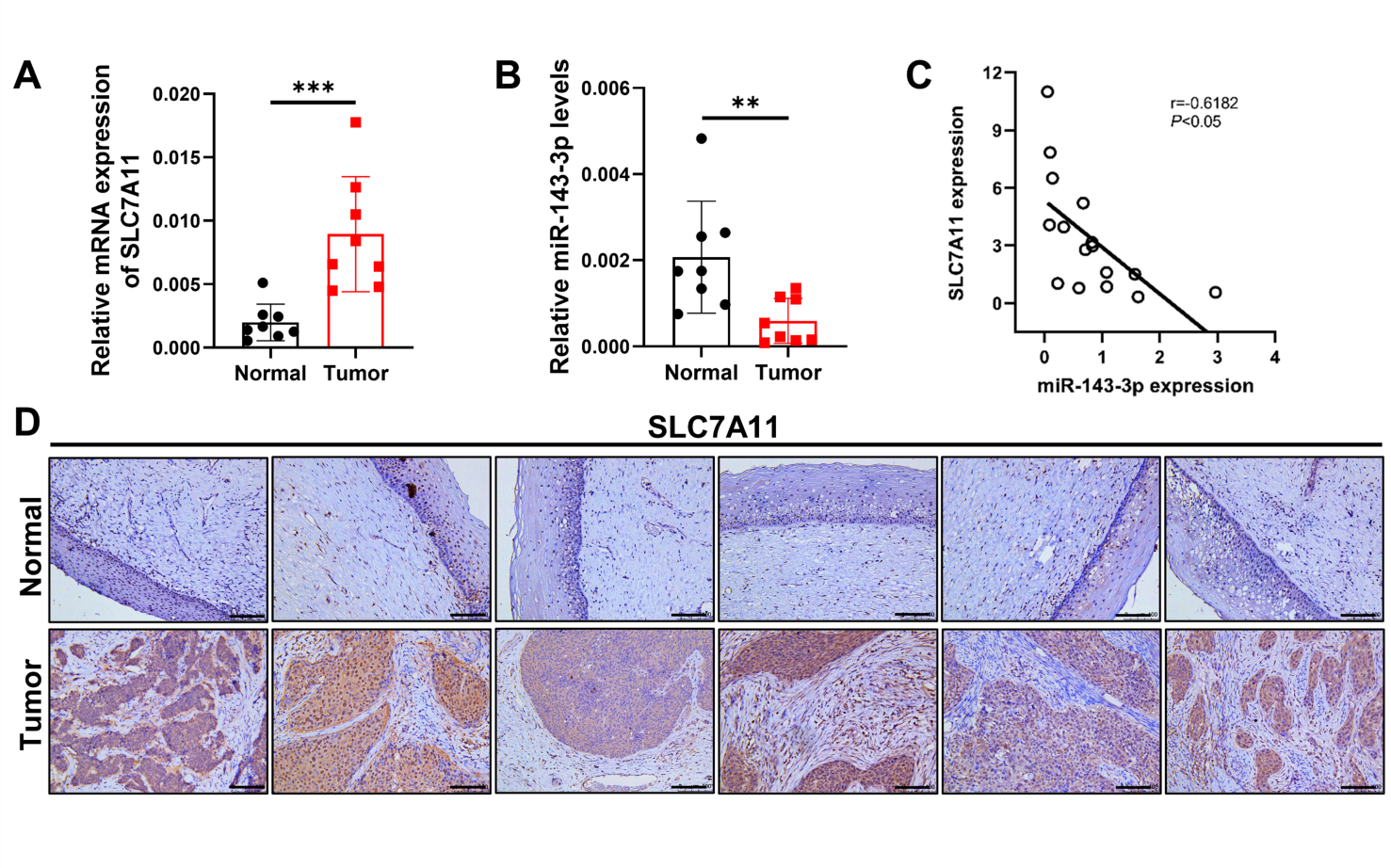


Figure 4

Expression of SLC7A11 and miR-143-3p in cervical squamous cell carcinoma (SCC) and normal cervical tissues. (A, B) Quantitative real-time PCR (qRT-PCR) analysis of SLC7A11 (A) and miR-143-3p (B) levels. (C) Correlation analysis between miR-143-3p and SLC7A11 expression. (D) Immunohistochemical staining of SLC7A11. Scale bars, as indicated. Data are presented as mean ± SD. **p < 0.01, ***p < 0.001.

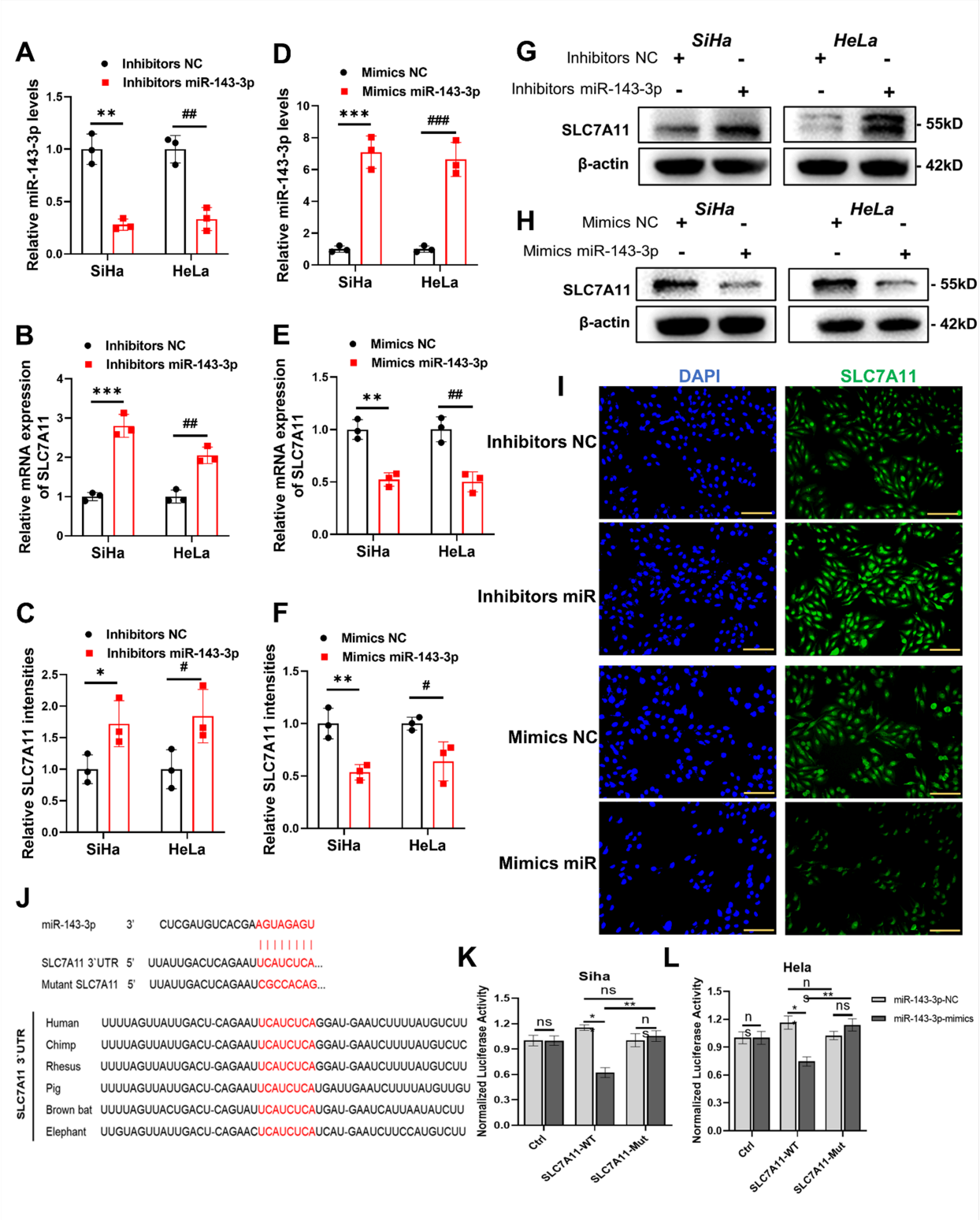


Figure 5

Figure 5. Functional validation of miR-143-3p–mediated regulation of SLC7A11 in cervical cancer cells. (A) Quantitative real-time PCR (qRT-PCR) analysis of miR-143-3p expression in SiHa and HeLa cells transfected with miR-143-3p inhibitors or negative control (NC). (B, C) qRT-PCR analysis of SLC7A11 mRNA expression and quantification of its protein levels following miR-143-3p inhibition. (D) qRT-PCR analysis of miR-143-3p expression in SiHa and HeLa cells transfected with miR-143-3p mimics or NC. (E,

F) qRT-PCR analysis of SLC7A11 mRNA levels and protein quantification following miR-143-3p overexpression. (G, H) Western blot analysis of SLC7A11 protein expression in SiHa and HeLa cells transfected with miR-143-3p inhibitors or NC (G) and miR-143-3p mimic (H); β-actin was used as a loading control. (I) Immunofluorescence staining of SLC7A11 (green) and nuclei (DAPI, blue) in SiHa cells after miR-143-3p inhibition or overexpression. Scale bars, as indicated. (J) Predicted miR-143-3p binding site within the 3' untranslated region (3'UTR) of human SLC7A11, including wild-type (WT) and mutant (Mut) sequences and cross-species conservation. (K, L) Dual-luciferase reporter assays exhibiting relative luciferase activity of WT or Mut SLC7A11 3'UTR constructs in SiHa (K) and HeLa (L) cells co-transfected with miR-143-3p mimics or NC. Data are presented as mean ± SD. *$p < 0.05$, **$p < 0.01$, ***$p < 0.001$; ns, not significant.

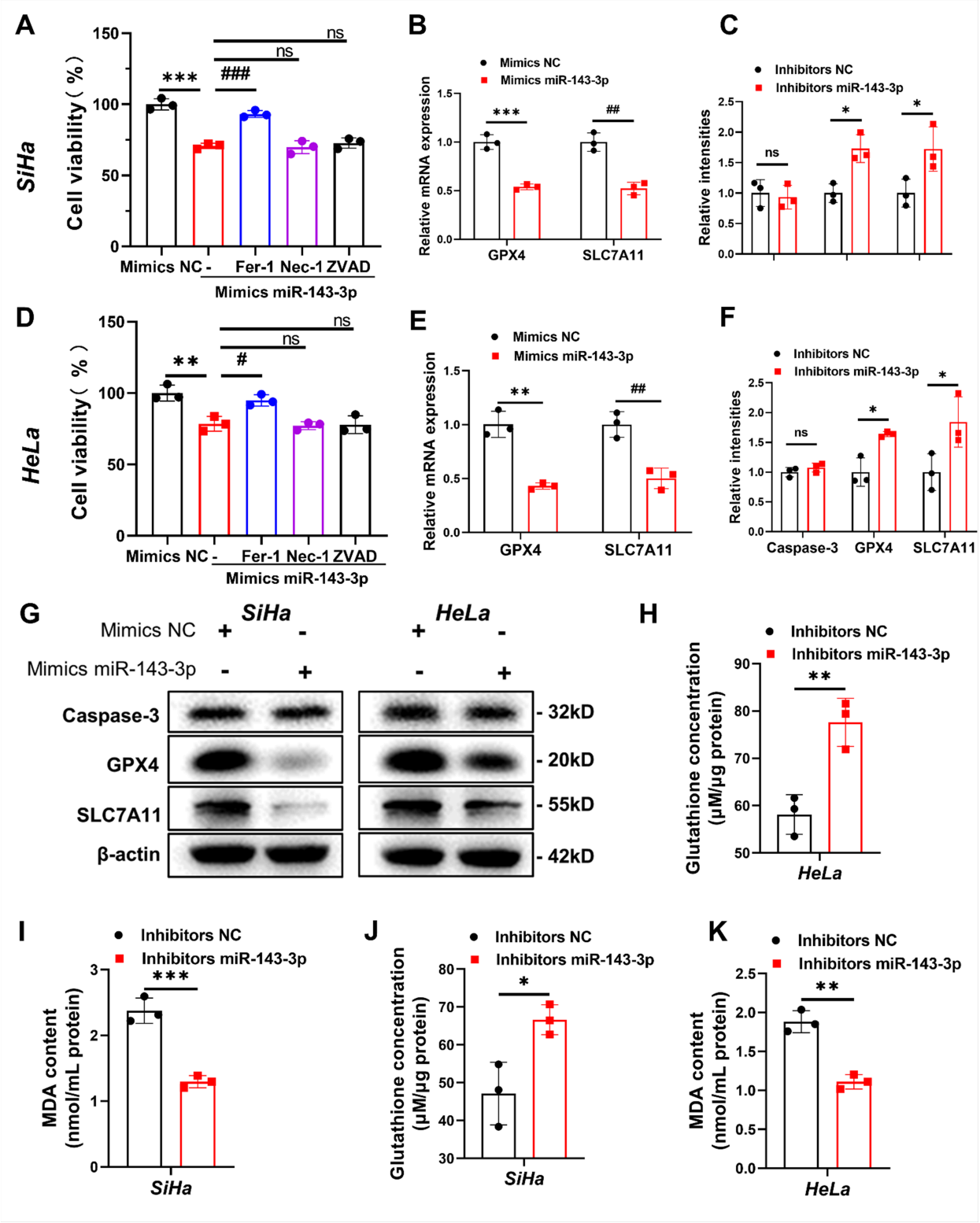


Figure 6

Effects of miR-143-3p on ferroptosis-related cell death in cervical cancer cells. (A, D) Cell viability of SiHa (A) and HeLa (D) cells transfected with miR-143-3p mimics or negative control (NC) following treatment with ferroptosis inhibitor Ferrostatin-1 (Fer-1), necroptosis inhibitor Necrostatin-1 (Nec-1), or Z-VAD-FMK (ZVAD) inhibitor of apoptosis, as indicated. (B, E) Quantitative real-time PCR (qRT-PCR) analysis of GPX4 and SLC7A11 mRNA expression in SiHa (B) and HeLa (E) cells in response to miR-143-

3p overexpression. (C, F) Relative protein levels of ferroptosis- and apoptosis-related markers in SiHa (C) and HeLa (F) cells after miR-143-3p inhibition. (G) Western blot analysis of Caspase-3, GPX4, and SLC7A11 protein expression in SiHa and HeLa cells transfected with miR-143-3p mimics or NC; β-actin was used as a loading control. (H–K) Intracellular glutathione (GSH) levels and malondialdehyde (MDA) content in HeLa (H, K) and SiHa (I, J) cells following miR-143-3p inhibition. Data are presented as mean ± SD. *p < 0.05, **p < 0.01, ***p < 0.001; ns, not significant.

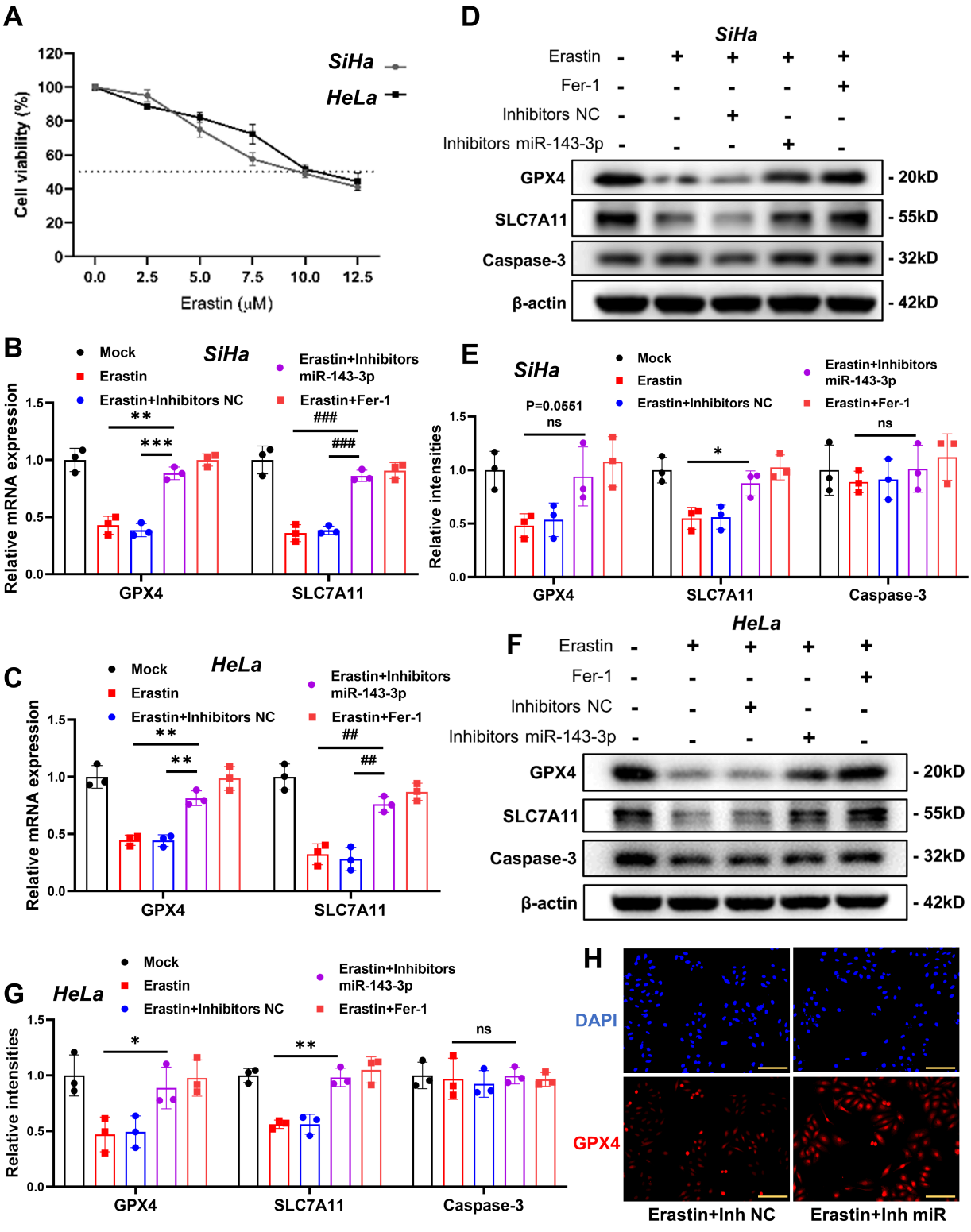


Figure 7

Effects of miR-143-3p on erastin-induced ferroptosis in cervical cancer cells.(A) Cell viability of SiHa and HeLa cells treated with increasing concentrations of erastin. (B, C) Quantitative real-time PCR (qRT-PCR) analysis of GPX4 and SLC7A11 mRNA expression in SiHa (B) and HeLa (C) cells subjected to mock conditions, erastin alone, erastin combined with miR-143-3p inhibitors or inhibitor negative control (NC), and erastin combined with Ferrostatin-1 (Fer-1), as indicated. (D–G) Western blot analysis and quantification of relative protein expression of GPX4, SLC7A11, and Caspase-3 in SiHa (D, E) and HeLa (F, G) cells treated with erastin in the presence or absence of miR-143-3p inhibitors or Fer-1; β-actin was used as a loading control. (H) Immunofluorescence staining of GPX4 (red) and nuclei (DAPI, blue) in SiHa cells treated with erastin and transfected with inhibitor NC or miR-143-3p inhibitors. Scale bars, as indicated. Data are presented as mean ± SD. *$p < 0.05$, **$p < 0.01$, ***$p < 0.001$; ns, not significant.

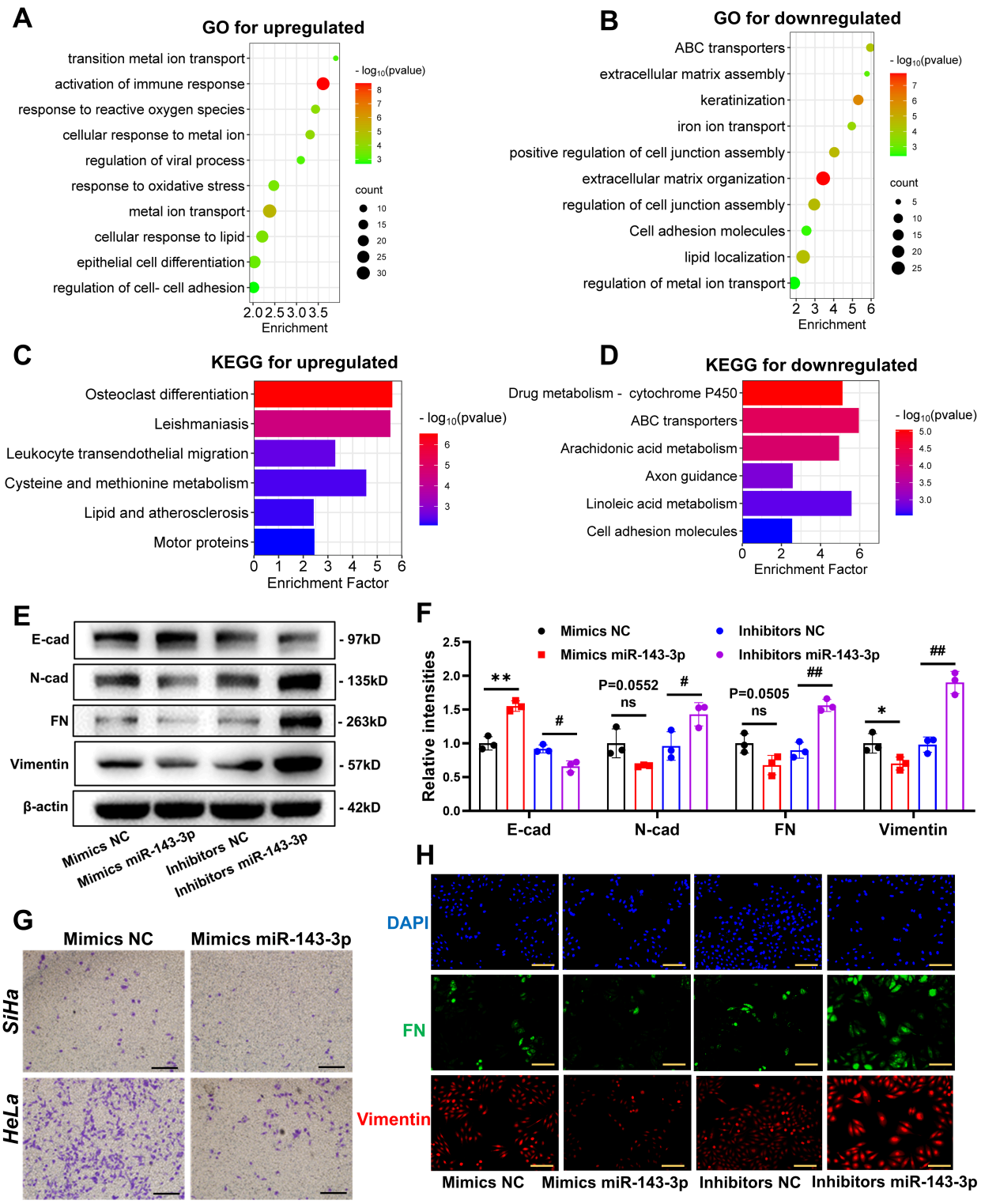


Figure 8

Effects of miR-143-3p on biological pathway enrichment and epithelial–mesenchymal transition (EMT)–related phenotypes in cervical cancer cells. (A, B) Gene Ontology (GO) functional analysis of upregulated (A) and downregulated (B) differentially expressed genes, highlighting significantly enriched biological processes. (C, D) Kyoto Encyclopedia of Genes and Genomes (KEGG) pathway enrichment analysis of upregulated (C) and downregulated (D) genes. Enrichment significance is indicated by

−log10(p-value), and dot size indicates gene counts where applicable. (E, F) Western blot analysis and quantification of EMT-related markers, including E-cadherin (E-cad), N-cadherin (N-cad), fibronectin (FN), and vimentin, in cervical cancer cells transfected with miR-143-3p mimics, inhibitors, or their respective negative controls (NCs); β-actin was used as a loading control. (G) Transwell migration assays of SiHa and HeLa cells following transfection with miR-143-3p mimics or NC. (H) Immunofluorescence staining of FN (green), vimentin (red), and nuclei (DAPI, blue) in cervical cancer cells transfected with miR-143-3p mimics or inhibitors and corresponding NCs. Scale bars, as indicated. Data are presented as mean ± SD. *p < 0.05, **p < 0.01; ns, not significant.

Supplementary Files

This is a list of supplementary files associated with this preprint. Click to download.

- UncroppedfulllengthWesternblotmembrane.pdf